DEUTSCHES ELEKTRONEN-SYNCHROTRON DESY

DESY SR 85-13
October 1985

DECAY OF THE GIANT 4d PHOTOABSORPTION RESONANCE IN ATOMIC Cs AND Sm

by

Th. Prescher, M. Richter, E. Schmidt, B. Sonntag, H.E. Wetzel

II. Inst. f. Experimentalphysik, Universität Hamburg

ISSN 0723-7979

NOTKESTRASSE 85 · 2 HAMBURG 52

To be sure that your preprints are promptly included in the
HIGH ENERGY PHYSICS INDEX ,
send them to the following address (if possible by air mail) :

DESY
Bibliothek
Notkestrasse 85
2 Hamburg 52
Germany

DESY SR 85-13
October 1985

ISSN 0723-7979

Decay of the giant 4d photoabsorption resonance in atomic Cs and Sm

Th. Prescher, M. Richter, F. Schmidt, B. Sonntag and H.E. Wetzel
II. Institut für Experimentalphysik der Universität Hamburg,
D-2000 Hamburg 50, Germany

Abstract

The photoelectron spectra and the relative partial photoionization cross sections of atomic Cs and Sm have been determined in the photon energy range of 4d - 4f, εf excitations (Cs 50 eV - 130 eV; Sm 120 eV - 160 eV). For Cs direct 4d ionization dominates whereas the Sm "4d → 4f, εf resonance" mainly autoionizes via the emission of a 4f electron. The Sm 4d partial cross section goes through a maximum 15 eV above threshold, where it becomes comparable to the 4f partial cross section. The 4f type character of the Sm excited wave function at threshold turns into 4f, εf type character 10 eV above. Close to the 4d threshold the 5s, 5p, and two electron satellite photoemission lines are strongly enhanced for both atoms.

to be published in J. Phys. B

1. Introduction

Solid rare earths (Gerken et al. 1982, Zimkina et al. 1967, Strasser et al. 1985) and atomic rare earths (Wolff et al. 1976, Mansfield and Connerade 1976, Radtke 1979, Connerade 1978, Becker et al. 1985) exhibit giant resonances above the 4d threshold, which gain their oscillator strength from transitions of 4d electrons into the partially unoccupied 4f shell (Starace 1972, Sugar 1972, Dehmer and Starace 1972, Wendin and Starace 1978, Zangwill and Soven 1980, Wendin 1982, Amusia et al. 1981). Xe, Cs, and Ba, the elements preceding the rare earths in the periodic table, also display strong absorption maxima above the 4d threshold (Ederer 1964, Haensel et al. 1969, Rabe et al. 1974, Connerade and Mansfield 1974, Hecht and Lindau 1981, Petersen et al. 1975, Starace 1982, Samson 1982, Amusia 1983, Kelly 1983, Zangwill 1983, Amusia 1985). On passing from Xe to elements with higher Z there is a systematic change of the strong absorption resonance. The maximum gets narrower and the main peak shifts towards threshold. The character of the excited electron wave function is expected to change from εf type (Xe, Cs, Ba) to "4f, εf" type (La - Tm). This is corroborated by the multiplet structure displayed by the absorption spectra. Determining the decay channels of the resonance forms an ideal method to probe the character of the excited state. For low Z elements the main process can be viewed as

$$4d^{10}4f^{N} \rightarrow 4d^{9}(4f\varepsilon f)^{N+1} \rightarrow 4d^{9}4f^{N} + \varepsilon\ell$$

whereas for high Z the process

$$4d^{10}4f^{N} \rightarrow 4d^{9}(4f\varepsilon f)^{N+1} \rightarrow 4d^{10}4f^{N-1} + \varepsilon\ell$$

dominates. The photoemission data on solid rare earths are consistent with this picture. Due to the considerable difficulties encountered in determining the VUV photoelectron spectra of free rare earth atoms, experimental results are scarce. Only very recently photoelectron spectra of atomic Lu taken in the energy range of the 4d excitations have been reported (Becker et al. 1985a). There are preliminary data on atomic Ba (Wuilleumier 1984, Becker et al. 1985b). In order to test the above ideas we investigated the photoelectron spectra of atomic Cs and Sm. In Cs $4d^{10}5s^{2}5p^{6}6s\ ^{2}S$ the 4f function is not collapsed even in the core excited state whereas in Sm $4d^{10}5s^{2}5p^{6}4f^{6}6s^{2}\ ^{7}F$ the 4f shell is collapsed and partially occupied. Therefore the change in

character of the resonance should show up very clearly. In this context we also wanted to examine to which extent the resonance decays via 5s, 5p, and 6s emission. A further point of interest was the strength and energy dependence of satellite emission.

2. Experiment

For the photoelectron measurements the synchrotron radiation emitted by the electron storage ring BESSY was used. Additional experiments were performed at the storage ring DORIS. In all cases the radiation was monochromatized by toroidal grating monochromators (BESSY: TGM1 bandwidth ΔE = 0.3 eV at $\hbar\omega$ = 70 eV; ΔE = 0.6 eV at $\hbar\omega$ = 105 eV, Gudat et al. 1982; TGM2 ΔE = 0.5 eV at $\hbar\omega$ = 80 eV; ΔE = 1.6 eV at $\hbar\omega$ = 140 eV, Braun et al. 1983; DORIS: TGM ΔE = 0.3 eV at $\hbar\omega$ = 80 eV; ΔE = 0.5 eV at $\hbar\omega$ = 140 eV, Bruhn et al. 1983). The monochromatic photon beam (approximately 10^{11} photons/s) was focused onto the interaction zone, where it crossed the atomic beam emanating from a resistively heated high temperature furnace. Temperatures around 415 K for Cs and 900 K for Sm are sufficient to attain a vapour pressure of 0.6 Pa in the furnace. The density of atoms in the interaction region is estimated to be $\sim 10^{12}$ atoms/cm^3. The kinetic energy of electrons emerging from the interaction zone was determined by a cylindrical mirror analyzer (angular acceptance 0.8 % of 4π, energy resolution ΔE = 0.8 % of the pass energy). Only electrons emitted at angles close to the magic angle of 54°44' relative to the polarization vector of the incoming light were accepted by the analyzer. The partial cross sections were determined from a series of photoelectron spectra taken at different photon energies and also from constant ionic final state spectra (CIS), where the photon energy and the pass energy of the electron energy analyzer were scanned simultaneously. All spectra were normalized to the incoming photon flux and corrected for the energy-dependent bandpass of the electron spectrometer. Since the density of atoms in the interaction zone could not be determined, only relative cross sections have been obtained. Instabilities of the atomic beam are the main source of the errors. Details of the experimental set-up are given elsewhere (Schmidt et al. 1984, Schröder 1982, Schmidt 1985).

3. Results and Discussion

3.1 Cs

photoelectron spectra

The photoelectron spectrum of atomic Cs taken at the maximum of the absorption resonance ($h\omega$ = 105 eV) (Petersen et al. 1975) is presented in Fig. 1. The 5p, 5s, and 4d photoelectron lines are clearly seen. The splitting of the Cs II $5p^5 6s\ ^3P$, ^1P; $5p^5 5d\ ^3P$ ^1D states (Süzer et al. 1980) is not fully resolved in the 105 eV spectrum. At $h\omega$ = 50 eV the $5p_{3/2}$ peak splits into two components. The Auger lines ($4d^{-1} \rightarrow 5s^{-1}5p^{-1}$, $4d^{-1} \rightarrow 5p^{-2}$; $4d^{-1} \rightarrow 5p^{-1}6s^{-1}$) extend from the low energy end of the spectrum up to 65 eV kinetic energy. Taking into account the lower energy resolution of our analyzer there is good agreement with the ejected electron spectrum reported by Aksela and Aksela (1983). The main photoelectron lines are accompanied by a host of satellite lines, marked S1 - S10 in Fig. 1. For photon energies between 88 eV and 102 eV the satellite lines S3, S4, S5, and S6 are hard to disentangle from the overlapping Auger lines. The 6s photoelectron line is very weak and much less intense than many of the satellite lines. The binding energies and our assignment of the photoelectron lines are summarized in Table 1. The assignment is based on tabulated energy values for atomic Cs (Reader 1976) and Ba (Moore 1958), the Z + 1 analogue to core excited Cs. The binding energies determined from these "optical data" are given for comparison.

partial cross sections

In Fig. 2 the Cs 5s, 5p, and 4d partial cross sections are presented. For comparison the absorption spectrum (Petersen et al. 1975) is included. Due to problems inherent to photographic recording and due to saturation effects the center part of the absorption spectrum could only be estimated. The absorption spectrum has been aligned with the 4d partial cross section at the high energy end. Due to the neglect of other ionization channels, this results in an absorption cross section somewhat to low. The close similarity between the absorption spectrum and the 4d-partial cross section corroborates the dominance of the direct $4d \rightarrow \varepsilon l$ ionization. Both the 5s and the 5p partial cross sections show a prominent maximum at 100 eV and a shoulder at ~ 93 eV. According to Hartree-Slater calculations (Theodosiou and Fielder 1982) these cross sections should smoothly decrease towards higher energies. The enhancement of the 5s and 5p partial cross sections is caused by the interaction of the 5s, 5p $\rightarrow \varepsilon l$ channels

with the 4d → εf channel. This intershell coupling has not been taken into account in the Hartree-Slater calculations. The 5s and 5p partial cross sections peak at photon energies well below the peak position of the main 4d channel. The characteristic features of the above results can be explained in terms of the local field model (Zangwill and Soven 1980, Zangwill 1983, Wendin 1982). Under the influence of the external electromagnetic field the 4d-shell oscillates like a damped harmonic oscillator. The resulting dipolar field is superimposed on the external field. Below resonance the 4d shell oscillates in phase with the external field giving rise to an enhancement of the local field outside the 4d-shell, i.e. in the range of the 5s and 5p shells.

Within the "Random Phase Approximation with Exchange" (RPAE) Amusia and coworkers (Amusia et al. 1976, Amusia and Cherepkov 1975, Amusia 1983, 1984) have calculated the Cs 5s, Cs(5s+5p), and 4d partial cross sections. For the 4d partial cross section it is essential that by generalization of RPAE they succeeded to take the relaxation of the electrons around the core hole into account (Amusia et al. 1976). The calculated cross sections are given in Fig. 2. The partial 5p cross section has been obtained by subtracting σ5s from σ(5s+5p). The experimental curves have been scaled by matching the experimental σ5p to the theoretical cross section for photon energies below 90 eV and at 110 eV. For σ4d there is reasonable agreement between theory and experiment. The theory overestimates the width of the resonance. The experimental 5s partial cross section is considerably smaller than the theoretical cross section and peaks at higher energies. A similar discrepancy has been noted for atomic Xe (Amusia 1982, 1984) and Ba (Zangwill and Soven 1980). The admixture of outer shell excited states (e.g., $5s^2 5p^4 nd\ 6s$, $5s^2 5p^4 6s\ nd$) to the $5s5p^6 6s$ state transfers oscillator strength to other channels and thus lowers the 5s cross section. For photon energies far above the 5s threshold the modified partial cross section is given by

$$\sigma_{5s}(\hbar\omega) = F_{5s}\sigma^0_{5s}(\hbar\omega)$$

where $\sigma^0_{5s}(\hbar\omega)$ denotes the cross section without allowing for this configuration interaction. The spectroscopic factor F_{5s} describes the weight of the $5s5p^6 6s\varepsilon l$ state. From our data we deduce $F_{5s} = 0.6$. For Xe a value of 0.3 has been determined (Amusia 1984). The gross features of the experimental σ_{5p} are well described by the theory. Towards higher photon energies the theoretical

curve decreases more steeply than the experimental one. The shoulders at about 93 eV in the experimental σ_{5s} and σ_{5p} spectra have no counterparts in the theoretical spectra. We attribute these shoulders to the simultaneous excitation of a 4d electron and a 5p electron. Similar structures due to these two electron excitations have been detected in the spectra of metallic Cs and solid and crystalline CsCl (Radler and Sonntag 1976). In the absorption spectrum of atomic Cs (Petersen et al. 1975) these transitions give rise to a series of lines between 93 eV and 100 eV. Autoionization of the two electron excited states should lead to an enhancement of the satellite emission. This is consistent with our results for the satellite intensities.

satellite emission

The satellite partial cross sections for the 4d-satellite (S2), the 5s-satellites (S3 - S7), and the 5p-satellites (S8, S9) are presented in Fig. 3. The experiment yields the partial satellite cross sections relative to the σ_{5p} cross section. By scaling σ_{5p} to the theoretical cross section the absolute satellite cross sections have been obtained. Between 90 eV and 100 eV photon energy Auger lines (Aksela and Aksela 1983) overlap some of the 5s-satellites, preventing an exact determination of their relative strength. All the 5s-, 5p-satellite cross sections peak in the same energy range (95 eV - 105 eV) as the partial 5s- and 5p-cross sections (see Fig. 2). This clearly demonstrates the coupling of the direct 5s, 5p → εl channels and the satellite channels. The 5p-satellites (S8, S9, S10, S11 only to be seen for $\hbar\omega \lesssim 55$ eV) are attributed to shake-up of the outer 6s electrons. This is consistent with the absence of satellite lines close to the 5p-photoelectron lines in the spectrum of atomic Xe (Adam et al. 1978, Fahlmann et al. 1984). The great number of $5s5p^6 nl$, $5s^2 5p^4 nl, n'l'$ final states renders the interpretation of the satellite lines close to the 5s line a very difficult task. There is some similarity to the Xe spectrum but the assignment of the Xe satellite lines only can be used for guidance. To the authors knowledge there are no energies for the $5s^2 5p^4 nl, n'l'$ states available in the literature . The states listed in Table 1 are to be understood as possible ionic final states. The energy separation of the satellite lines S1 and S2 from the 4d lines suggests an interpretation in terms of $4d^{10}5s^2 6s \rightarrow 4d^9 5s^2 5p^6 7s\varepsilon l$ shake-up transitions. The partial cross section of line S2 closely resembles the partial 4d-cross section.

branching ratios

The ratios of the partial cross sections of subshells with the same angular momentum ℓ but different total angular momentum $j = \ell + 1/2$ and $\ell - 1/2$ have been shown to dramatically deviate from the statistical ratio (Samson 1982, Krause et al. 1981, Ong and Manson 1980, Johnson and Cheng 1979, Banna et al. 1979). These deviations are very sensitive to relativistic and correlation effects (Ong and Manson 1980, Johnson and Cheng 1979). Measurements of these branching ratios therefore provide stringent tests for the theory. Branching ratios can be determined directly from the intensity of the spin-orbit split photoelectron lines registered at the same photon energy. Therefore there is no need for normalization to the incoming photon flux, only the small change in the bandpass of the electron energy analyzer has to be corrected for. This considerably reduces the uncertainties in the determination of relative partial cross sections. The experimental $\sigma 5p_{3/2} : \sigma 5p_{1/2}$ branching ratio in Cs is presented in Fig. 4. By looking at Fig. 4 and at Fig. 2 it becomes obvious that the energy dependence of the branching ratio cannot be explained by the kinetic energy effect. This effect predicts the branching ratio to be larger or smaller than the statistical ratio depending on whether the partial cross section is rising or falling as a function of energy (Walker et al. 1973, Walker and Waber 1974). The general features of the Cs branching ratio are similar to the Xe branching ratio (Krause et al. 1981, Johnson and Cheng 1979, Schmidt 1985). At low energies the branching ratio lies well below the statistical value. Towards higher energies it smoothly increases reaching a maximum value of 2.1 at 79 eV. Between 80 eV and 110 eV the branching ratio rapidly oscillates with low values at the 4d threshold and maxima at ~ 86 eV and 100 eV. The structure reminds one of the maximum and the shoulder displayed by the partial 5p cross section (see Fig. 2). This indicates the importance of intershell correlation. For Xe, Johnson and Cheng (1979) have shown that relativistic effects and the correlation between the 5s, 5p, and 4d shell are essential for explaining the energy dependence of the 5p branching ratio. This similarity to the Xe branching ratio is even more pronounced for the $\sigma 4d_{5/2} : \sigma 4d_{3/2}$ branching ratio given in Fig. 5 (Banna et al. 1979, Schmidt 1985, Yates et al. 1985). From a threshold value far above the statistical ratio the Cs branching ratio steeply drops reaching a minimum at ~ 98 eV. Towards higher photon energies this minimum is followed by a maximum at ~ 100 eV and a further minimum at 105 eV. Up to 160 eV the branching ratio stays below the statistical value. Again an interpretation in terms of the kinetic energy effect fails. For Xe the

gross features of the experimental 4d branching ratio are well described by results obtained by Cheng and Johnson (1983) within the relativistic random phase approximation (RRPA).

3.2 Sm

photoelectron spectra

Photoelectron spectra of atomic Sm taken below the giant $4d \rightarrow 4f\varepsilon f$ resonance ($\hbar\omega$ = 132.2 eV), at the first ($\hbar\omega$ = 134.6 eV) and above the second peak ($\hbar\omega$ = 154 eV) of the resonance are shown in Fig. 6. The weak line (16) at the low energy end (E_B = 5.7 eV) is due to the emission of a 6s electron. The two dominant lines (14, 15) are caused by Sm $4f^6 6s^2\ ^7F \rightarrow 4f^5 6s^2\ ^6H\ ^6F$ (E_B = 9.2 eV), ^6P (E_B = 11.9 eV)εl transitions. The binding energies are in agreement with those reported by Lee et al. (1977). Due to the limited energy resolution the splitting of the $4f^6 6s\ ^8F$, ^6F and the $4f^5 6s^2\ ^6H\ ^6F$ levels detected in the He I and Ne I photoelectron spectra (Lee et al. 1977) could not be resolved. The strong 4f emission lines are replicated by satellite lines (11,12) (E_B = 16.3, 19.0 eV) which in analogy to Cs we tentatively ascribe to $4f^6 6s^2\ ^7F \rightarrow 4f^5 6s 7s\ ^6H$, ^6F; $^6P\varepsilon l$ shake-up excitations. Sm $5p^6 4f^6 6s^2 \rightarrow 5p^5 4f^6 6s^2 \varepsilon l$ transitions give rise to the group of lines (7, 8, 9, 10) with 25 eV $\leq E_B \leq$ 32 eV. The splitting is caused by 5p spin-orbit interaction and the coupling of the open 5p and 4f shells. Satellite emission contributes to the high energy tail of this group (5, 6). Two 5s photoelectron lines (3, 4) clearly show up above 45 eV. The splitting is attributed to the interaction of the partly filled 4f and 5s shells. The peak separation of 3 eV is in good agreement with the value given for the 5s exchange splitting of Sm metal (Herbst et al. 1977). For photon energies above 140 eV the 4d emission lines (1, 2) (E_B = 130; 135.5 eV) could be well observed. The binding energies and the assignment of the photoelectron lines shown in Fig. 6 are summarized in Table 2.

partial cross sections

The photoelectron spectra (Fig. 6) already demonstrate the strong dependence of the intensity of the various photoelectron lines on the photon energy. Even more convincing is the resonant enhancement of the partial 4d, 5p and 4f cross sections in the range of the $4d^{10} 4f^6 6s^2 \rightarrow 4d^9 4f^7 6s^2$ excitations

displayed in Fig. 7. By adding all partial cross sections the uppermost curve in Fig. 7 has been obtained. This curve resembles the absorption spectrum reported by Radtke (1979). In the absorption spectrum the maximum at 145 eV is less pronounced. This may be due to the limited dynamic range of photographic plates used in the absorption measurements. In analogy to the interpretation of the 4d absorption spectra of several rare earths (Sugar 1972, Wolff et al. 1976) we ascribe the structure to the multiplet splitting of the $4d^9 4f^7 6s^2$ configuration. Spectra recently calculated by using the atomic physics code RCN/RGG (Cowan 1981) display two groups of strong lines separated by ~ 8 eV (Kerkhoff 1985). Our results help to shed some light on the character of the final states. The weak maxima at $\hbar\omega$ = 127.5 eV, 130 eV and the dominant maximum close to the 4d-thresholds almost exclusively decay via $4d^9 4f^7 6s^2 \rightarrow 4d^{10} 4f^5 6s^2 \varepsilon l$ autoionisation. The interference between the discrete excitation plus autoionisation and the direct $4f^6 6s^2 \rightarrow 4f^5 6s^2 \varepsilon l$ ionisation causes the asymmetry in the Fano type profile of the 4f partial cross section. A tentative fit by a single Fano profile (Fano 1961)

$$\sigma = \sigma_a \frac{(q+\varepsilon)^2}{1+\varepsilon^2} + \sigma_b$$

with

$$\varepsilon = \frac{2(E-E_o)}{\Gamma}$$

results in:

resonance energy E_o = 133.4 eV
halfwidths Γ = 4.7 eV
asymmetry parameter q = 1.78

From our data we conclude that, for the $4d^9 4f^7 6s^2$ levels giving rise to the three low energy maxima, the 4f final state wave function is localized within the inner well of the effective potential (Wendin and Starace 1978) and has a large overlap with the 4d wavefunction. The escaping chance into the $4d^9 4f^6 6s^2 \varepsilon l$ continuum is very small. These low energy excitations are also coupled to the 5p ionisation channel. Because the 5p ionisation cross section is very small $\geq$ 100 eV above threshold, interference effects are less important. This is corroborated by the symmetric line shapes displayed by the 5p partial cross section. Our findings so far are consistent with recent theoretical (Amusia et al. 1981) and experimental (Becker et al. 1985a) results for atomic Eu.

The character of the final state responsible for the maximum centered at 145 eV, i.e. 10 eV above the $4d_{3/2}$ ionisation threshold, is completely different. There is only weak coupling to the 4f and 5p ionisation continua, causing the small bumps located at 141.5 eV in the 4f and 5p partial cross sections. The dominant decay of the 145 eV resonance leads to an $4d^9 4f^6 6s^2 \varepsilon l$ final state. This indicates that the f symmetric final state wavefunction is best described as an εf continuum wavefunction with strong 4f character close to the nucleus. The 4d-4f exchange interaction pushes part of the $4d \rightarrow 4f$ oscillator-strength far up above the ionisation limit. The character of the final state could be viewed upon as an f symmetric continuum resonance reflecting the structure of the effective potential (Wendin and Starace 1978). In this regard there is similarity to the situation encountered for the 4d excitation of atomic Cs. But due to the contracted nature of the 4f orbital, in Sm we encounter both, a localized 4f resonance close to the threshold and a εf 4f continuum resonance 10 eV above threshold whereas for Cs there is only the continuum εf resonance 20 eV above threshold. The characteristic results for atomic Sm are very similar to those determined in photoemission experiments on solid rare earths (Gerken 1983, Gerken et al. 1984).

Acknowledgement

The authors acknowledge the support of the BESSY and HASYLAB staff. Work supported by the Bundesministerium für Forschung und Technologie of the Federal Republic of Germany.

References

Adam M Y, Wuilleumier F, Sandner N, Schmidt V, and Wendin G 1978 J. Phys. (Paris) 39 129

Aksela H and Aksela A 1983 Phys. Rev. A28 2851

Amusia M Ya 1983 Atomic Physics 8 eds. I. Lindgren, A. Rosén, and S. Svanberg (Plenum Press, New York) p. 287

Amusia M Ya 1984 Proc. of the X-84 Internat. Conf. "X-Ray and Inner-Shell Processes in Atoms, Molecules and Solids" eds. A. Meisel, J. Finster, Karl-Marx-Univ. Leipzig p. 33

Amusia M Ya and Cherepkov N A 1975 Case Studies in Atomic Physics 5 47

Amusia M Ya, Ivanov V K, and Chernysheva L V 1976 Phys. Letters 3 191

Amusia M Ya, Sheftel S I, and Chernysheva L V 1981 Sov. Phys. Tech. Phys. 26 1444

Banna M S, Krause M O, and Wuilleumier F 1979 J. Phys. B12 L125

Becker U, Kerkhoff H G, Ferret T A, Heinmann P A, Kobrin P H, Lindle D W, Truesdale C M, and Shirley D A 1985a Phys. Rev. Lett. to be published

Becker U, Hölzel R, Kerkhoff H G, Langer B, Szostak D, und Wehlitz R 1985b Proc. XIV ICPEAC Stanford

Braun W, Jäkisch G, Baalmann A, and Radlik W 1983 BESSY Annual Report Berlin

Bruhn R, Schmidt E, Schröder H, Sonntag B, Thevenon A, Passereau G, and Flamand J 1983 Nucl. Instr. and Meth. 208 771

Cheng K T and Johnson W R 1983 Phys. Rev. A28 2830

Connerade J P 1978 Contemp. Phys. 19 415

Connerade J P and Mansfield M W D 1974 Proc. Roy. Soc A341 267

Cowan R D 1981 The Theory of Atomic Structure and Spectra (Berkeley: University of California Press)

Dehmer J L and Starace A F 1972 Phys. Rev. B5 1792

Ederer D L 1964 Phys. Rev. Lett 13 760

Fahlmann A, Krause M O, Carlson Th A, and Svensson A 1984 Phys. Rev. A30 812

Fano U 1961 Phys. Rev. 124 1866

Gerken F, Barth J, and Kunz C 1982 in Proc. of the Internat. Conf "X-ray and Inner-Shell Physics" ed. B. Crasemann, AIP Conf. Proc. No 94 (AIP New York) and references therein, p. 602

Gerken F 1983 thesis Universität Hamburg Int. Ber. DESY F 41 HASYLAB 83-03

Gudat W, Kisker E, Depautex C, and Rothberg G M 1982 Nucl. Instr. and Meth. 195 233

Haensel R, Keitel G, Schreiber P, and Kunz C 1969 Phys. Rev. 188 1375

Hecht M H and Lindau I 1981 Phys. Rev. Lett. 47 821

Herbst J F, Watson R E, and Baer Y 1977 Phys. Rev. B16 2447

Johnson W R and Cheng K T 1979 Phys. Rev. A20 978

Kelly H P 1983 Atomic Physics 8 eds. I. Lindgren, A. Rosén and S. Svanberg (Plenum Press, New York) p. 305

Kerkhoff H G 1985 private communication

Lee S T, Süzer S, Matthias E, Rosenberg R A, and Shirley D A 1977 J. Chem. Phys. 66 2496

Krause M O, Carlson Th A, and Woodruff P R 1981 Phys. Rev. A24 1374

Mansfield M W D and Connerade J P 1976 Proc. Roy. Soc. A352 125

Moore Ch E 1958 Atomic Energy Level Vol III, Circular of the Nat. Bureau of Standards 467 Washington

Ong W and Manson St 1980 Phys. Rev. A21 642

Petersen H, Radler K, Sonntag B, and Haensel R 1975 J. Phys. B8 31

Rabe P, Radler K, and Wolff H W 1974 in Vacuum UV Radiation Physics ed. E.E. Koch, R. Haensel, and C. Kunz (Vieweg-Pergamon, Berlin) p. 247

Radler K and Sonntag B 1976 Chem. Phys. Lett. 2 371

Radtke E R 1979 J. Phys. B12 L71, L77

Reader J 1976 Phys. Rev. A13 507

Samson J A R 1982 in Handbuch der Physik Vol 31 Springer Verlag Berlin Heidelberg p. 123

Schmidt E 1985 Thesis University of Hamburg

Schmidt E, Schröder H, Sonntag B, Voss H, and Wetzel H E 1984 J. Phys. B17 707

Schröder H 1982 Thesis University of Hamburg

Starace A F 1972 Phys. Rev. B5 1773

Starace A F 1982 in Handbuch der Physik Vol 31 Springer Verlag Berlin Heidelberg p. 1

Strasser G, Rosina G, Matthew J A D, and Netzer F P 1985 Journal of Phys. F15 739

Sugar J 1972 Phys. Rev. B5 1985

Süzer S, Breuckmann B, Menzel W, Theodosiou C E, and Mehlhorn W 1980 J. Phys. B13 2061

Theodosiou C E and Fielder W 1982 J. Phys. B15 4113

Walker T E H, Berkowitz J, Dehmer J L, and Waber J T 1973 Phys. Rev. Lett. 31 678

Walker T E H and Waber J T 1974 J. Phys. B7 674

Wendin G 1982 in X-Ray and Atomic Inner-Shell Physics 1982 ed. B. Crasemann AIP Conf. Proc. No 94 New York p. 495

Wendin G and Starace A F 1978 J. Phys. B11 4119

Wolff H W, Bruhn R, Radler K, and Sonntag B 1976 Phys. Lett. 59A 67

Wuilleumier F J 1984 Proc. of the X-84 Internat. Conf "X-Ray and Inner-shell Processes in Atoms, Molecules and Solids" eds. A. Meisel, J. Finster Karl-Marx-Univ. Leipzig p. 61

Yates B W, Tan K H, Coatsworth L L, and Bancroft G M 1985 Phys. Rev. A31 1329

Zangwill A 1983 Atomic Physics 8 eds. I. Lindgren, A. Rosén, and S. Svanberg (Plenum Press, New York) p. 339

Zangwill A and Soven P 1980 Phys. Rev. Lett. 45 204

Zimkina T M, Fomichev V A, Gribovskii S A, and Zhukova I I 1967 Sov. Phys. Solid State 9 1128

Table 1

Experimental binding energies E_B of the states of CsII giving rise to the photoelectron lines in figure 1. For comparison binding energies reported by Reader (1976) (*) and Aksela and Aksela (1985) (+) are given. The other values have been determined from optical data (Moore 1958). The energy of the $5p_{1/2}6s$ J = 1 state has been used for calibration.

	E_B (eV)			
line no.	this experiment	optical data	state of CsII	
S1	89.9 ± 0.40	89.99	$4d^9_{3/2}5s^25p^67s$	
S2	87.6 ± 0.80	87.70	$4d^9_{5/2}5s^25p^67s$	
	84.8 ± 0.3	85.07+	$4d^9_{3/2}5s^25p^66s$	
	82.5 ± 0.3	82.70+	$4d^9_{5/2}5s^25p^66s$	
S3	38.83 ± 0.2	38.80	$5s5p^69s$	
S4	37.71 ± 0.15	37.82	$5s5p^68s$	
S5	36.82 ± 0.15	36.64;36.67	$5s5p^54f$	$5s^25p^4nln'l'$
S6	35.75 ± 0.15	35.91	$5s5p^67s$	
S7	33.14 ± 0.15	33.17;33.38	$5s5p^66p$	
	30.66 ± 0.15		$5s5p^66s$	
S8	24.16 ± 0.25	24.10-24.12*	$5p^5_{1/2}7s$	
S9	22.40 ± 0.20	22.39-22.44*	$5p^5_{3/2}7s$	
S10	21.63 ± 0.35	21.44-21.81*	$5p^5_{1/2}6p$	
S11	19.90 ± 0.2	19.58-20.40*	$5p^5_{3/2}6p$	(observed at $\hbar\omega$ = 50 eV)
		19.14*	$5p^5_{1/2}6s$	J = 1
	17.6 ± 0.1	17.65*	$5p^5_{3/2}6s$	J = 1
	17.2 ± 0.1	17.31*	$5p^5_{3/2}6s$	J = 2

Table 2

Experimental binding energies E_B of the states of Sm II giving rise to the photoelectron lines in Fig. 6.

line no.	E_B (eV)	state of Sm II
1	135.5 ± 0.2	$4d^9{}_{3/2}5s^25p^64f^66s^2$
2	130.7 ± 0.2	$4d^9{}_{5/2}5s^25p^64f^66s^2$
3	48.2 ± 0.2	$5s5p^64f^66s^2$
4	45.2 ± 0.2	$5s5p^64f^66s^2$
5	37.9 ± 0.2	
6	34.0 ± 0.2	
7	31.4 ± 0.2	$5p^5{}_{1/2}4f^66s^2$
8	29.4 ± 0.2	$5p^5{}_{1/2}4f^66s^2$
9	26.9 ± 0.2	$5p^5{}_{3/2}4f^66s^2$
10	25.3 ± 0.2	$5p^5{}_{3/2}4f^66s^2$
11	19.0 ± 0.2	$4f^56s7s\ {}^6P$
12	16.3 ± 0.2	$4f^56s7s\ {}^6H\,{}^6F$
13	14.2 ± 0.2	
14	11.9 ± 0.1	$4f^56s^2\ {}^6P$
15	9.2 ± 0.1	$4f^56s^2\ {}^6H\ {}^6F$
16	5.7 ± 0.1	$4f^66s\ {}^8I\ {}^6I$

Figure Captions

Figure 1 Photoelectron spectrum of atomic Cs taken at a photon energy of 105 eV.

Figure 2 Experimental relative 5s (+), 5p (◇), and 4d (Δ) partial cross sections of atomic Cs. The experimental relative absorption cross section (Petersen et al. 1975) is shown for comparison. The absolute scale refers to the calculated 5s (–), 5p (–·–·–), and 4d (– – –) partial cross sections (Amusia et al. 1975, 1976).

Figure 3 Partial satellite cross sections for atomic Cs. (S3 + S4 + S5) and (S8 + S9) give the cross section for the group of lines. The absolute cross section scale has been established by matching the experimental 5p partial cross section to the calculated cross section (Amusia et al. 1975).

Figure 4 $\sigma 5p_{3/2}/\sigma 5p_{1/2}$ branching ratio in atomic Cs.

Figure 5 $\sigma 4d_{5/2}/\sigma 4d_{3/2}$ branching ratio in atomic Cs.

Figure 6 Photoelectron spectra of atomic Sm taken at photon energies below ($\hbar\omega$ = 132.2 eV), at ($\hbar\omega$ = 134.6) and above ($\hbar\omega$ = 154.0 eV) the 4d → (4fεf) resonance.

Figure 7 Experimental relative 5p, 4d, and 4f partial cross sections of atomic Sm. The uppermost curves represent the sum of the partial cross sections.

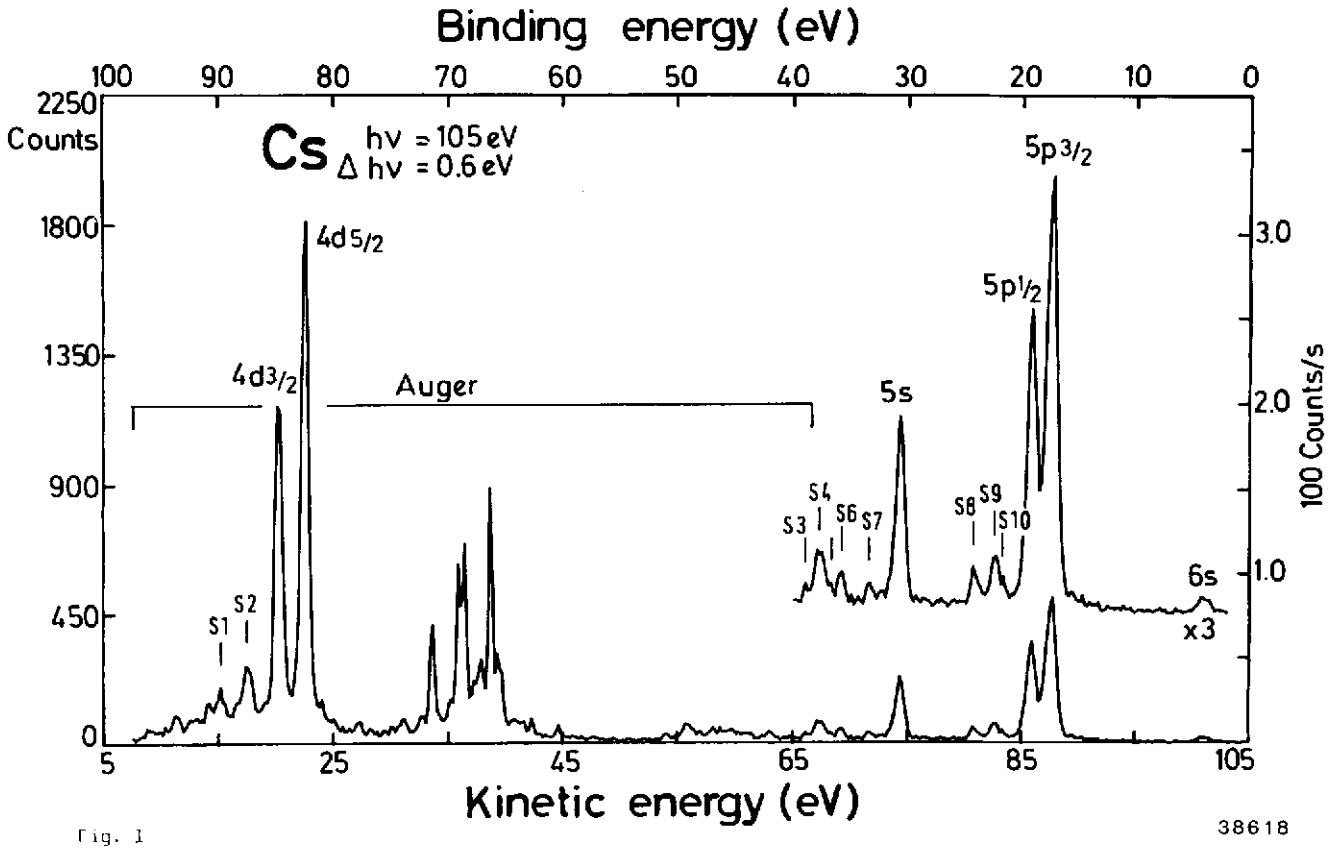

Fig. 1

38618

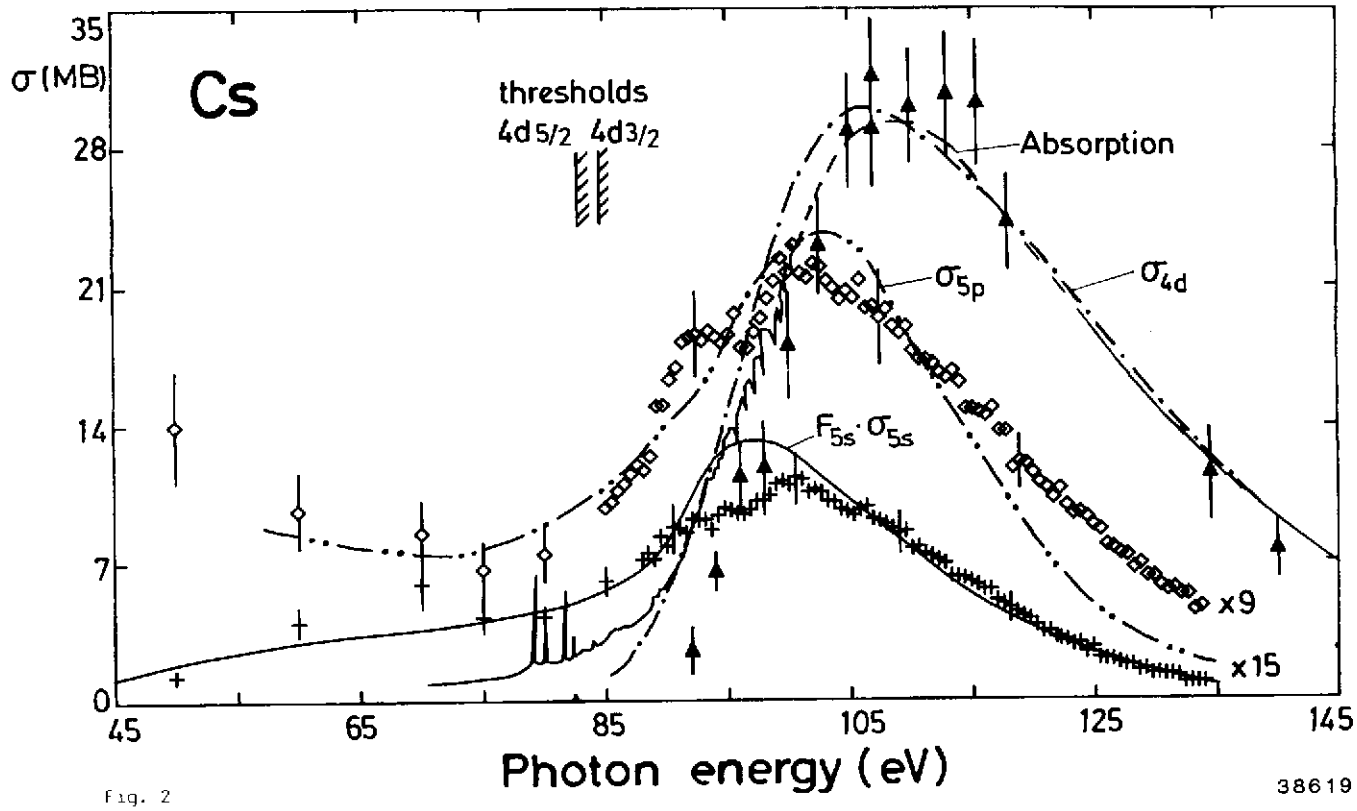

Fig. 2

38619

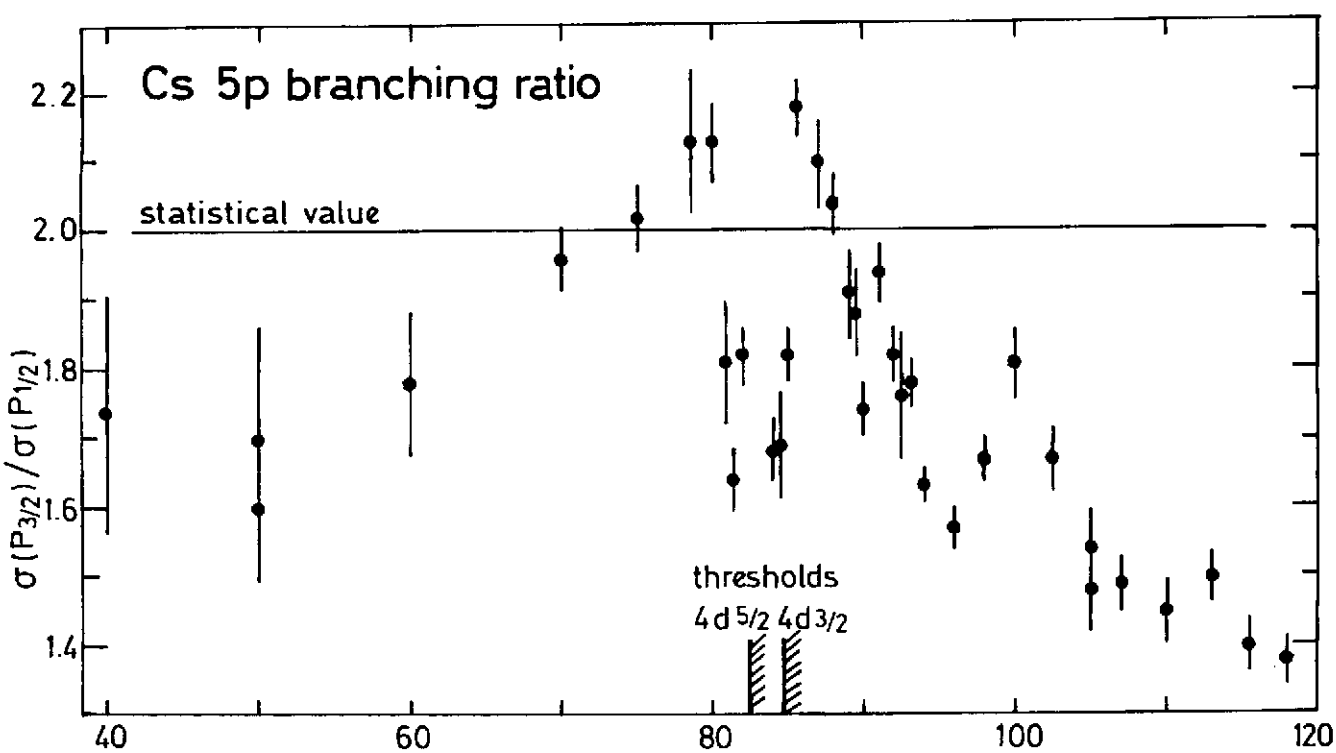

Fig. 4

38617

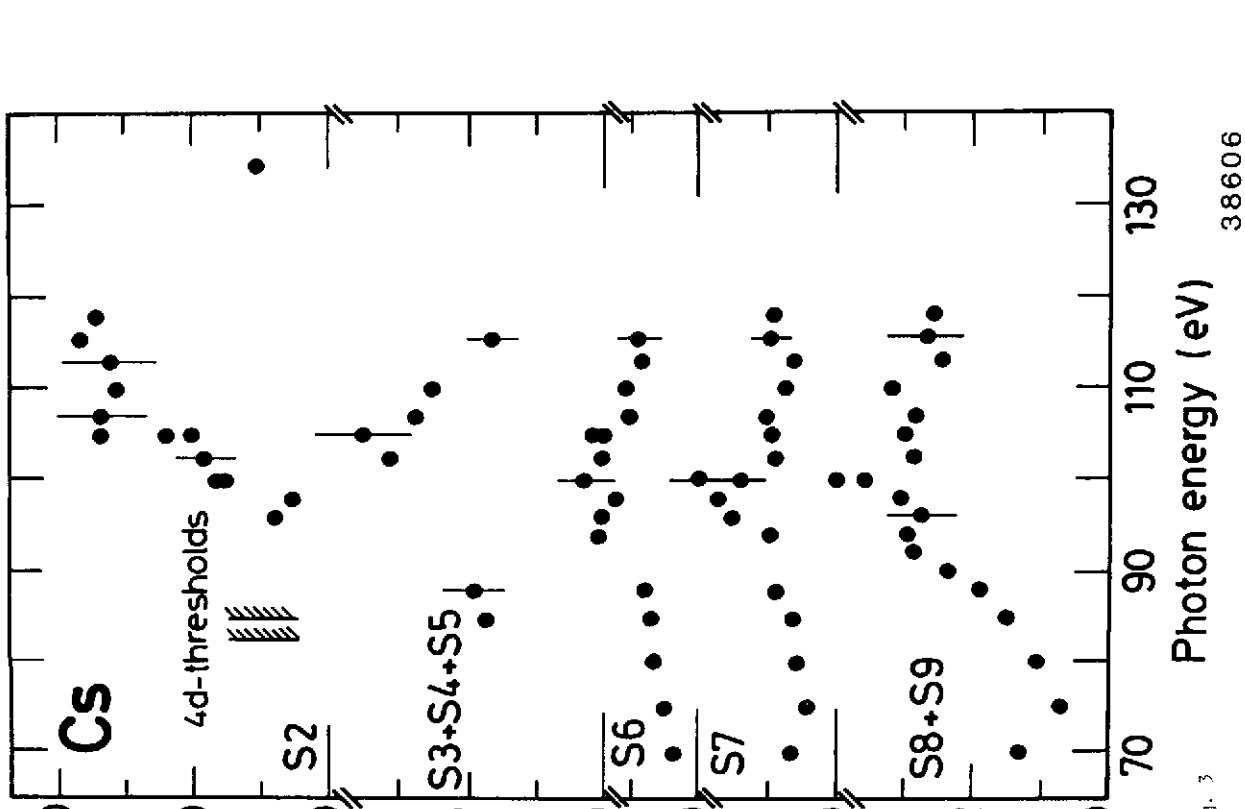

Fig. 3

38606

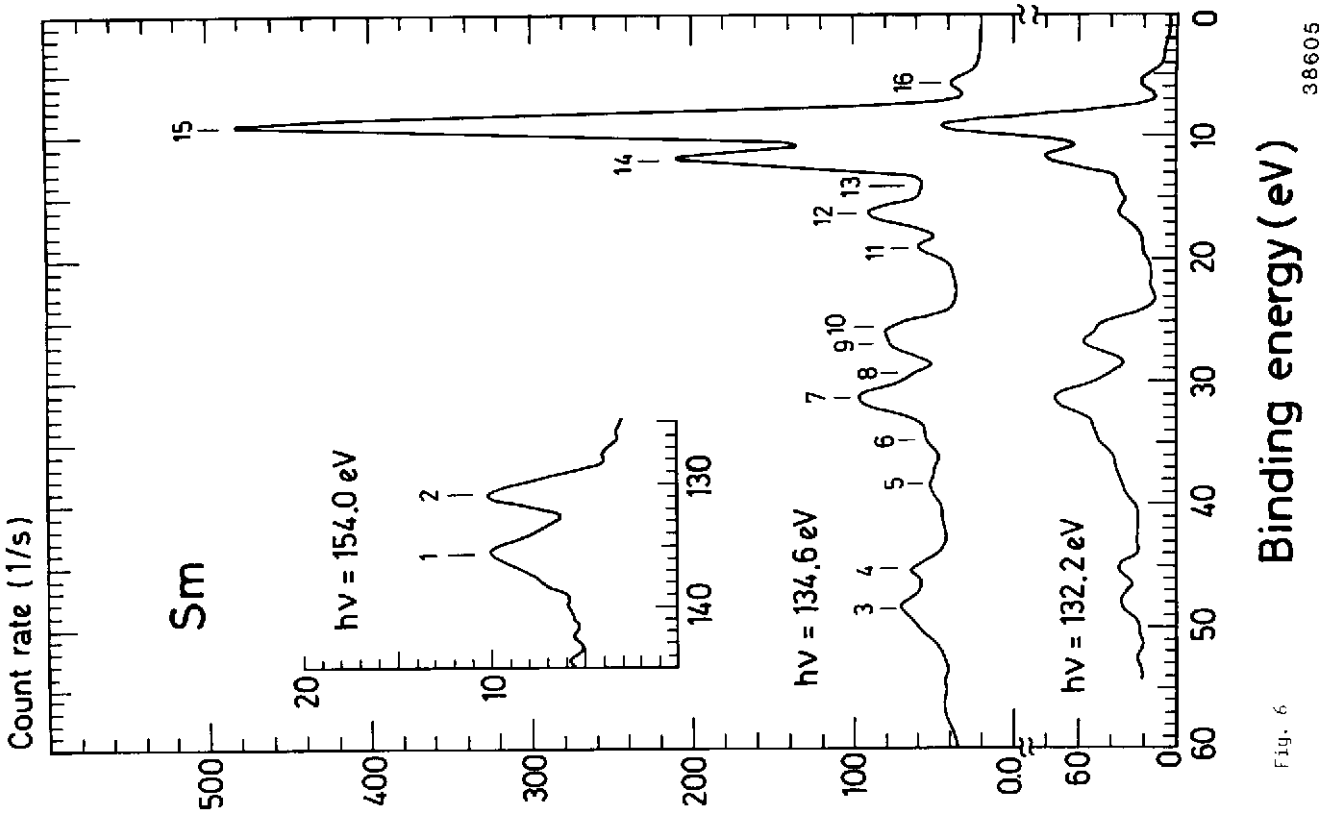
Count rate (1/s)
Sm
hν = 154.0 eV
hν = 134.6 eV
hν = 132.2 eV
Binding energy (eV)
38605

Fig. 6

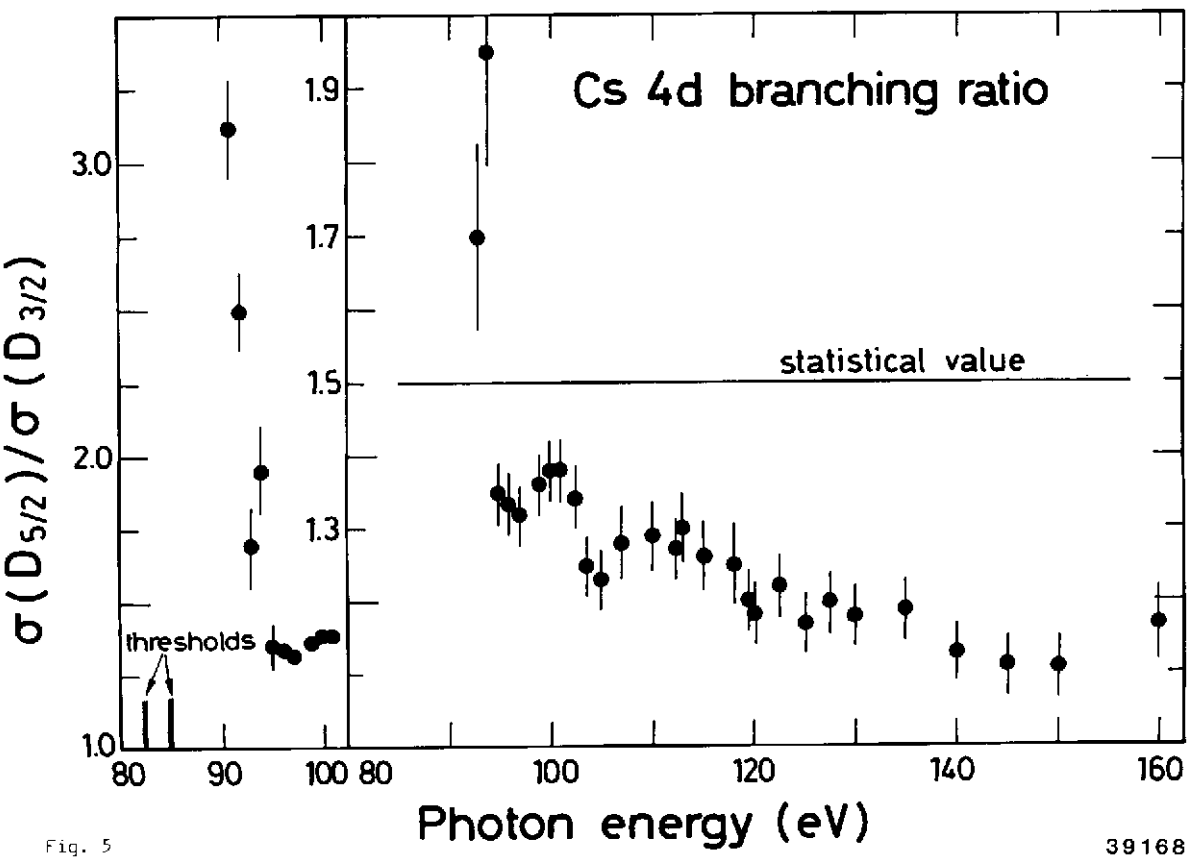
Cs 4d branching ratio
statistical value
thresholds
σ(D5/2)/σ(D3/2)
Photon energy (eV)
39168

Fig. 5

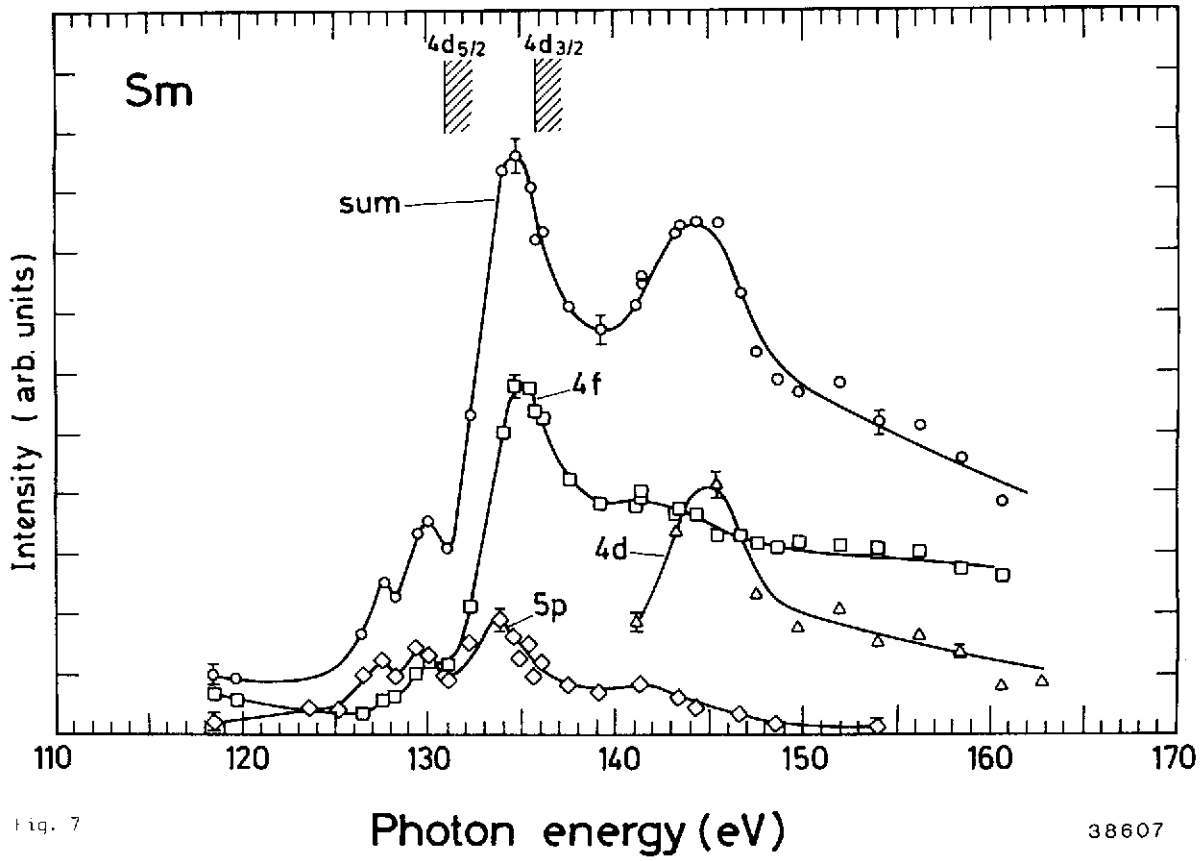
Sm
4d5/2
4d3/2
sum
4f
4d
5p
Intensity (arb. units)
110
120
130
140
150
160
170
Photon energy (eV)

Fig. 7

38607